

# Anharmonic resonance absorption of short laser pulses in clusters: A molecular dynamics simulation study

S. S. Mahalik and M. Kundu

*Institute for Plasma Research, HBNI, Bhat, Gandhinagar - 382 428, Gujarat, India*

(Dated: December 8, 2016)

Linear resonance (LR) absorption of an intense 800 nm laser light in a nano-cluster requires a long laser pulse  $> 100$  fs when Mie-plasma frequency ( $\omega_M$ ) of electrons in the expanding cluster matches the laser frequency ( $\omega$ ). For a short duration of the pulse the condition for LR is not satisfied. In this case, it was shown by a model and particle-in-cell (PIC) simulations [Phys. Rev. Lett. 96, 123401 (2006)] that electrons absorb laser energy by anharmonic resonance (AHR) when the position-dependent frequency  $\Omega[r(t)]$  of an electron in the self-consistent anharmonic potential of the cluster satisfies  $\Omega[r(t)] = \omega$ . However, AHR remains to be a debate and still obscure in multi-particle plasma simulations. Here, we identify AHR mechanism in a laser driven cluster using molecular dynamics (MD) simulations. By analyzing the trajectory of each MD electron and extracting its  $\Omega[r(t)]$  in the self-generated anharmonic plasma potential it is found that electron is outer ionized *only* when AHR is met. An anharmonic oscillator model, introduced here, brings out most of the features of MD electrons while passing the AHR. Thus, we not only bridge the gap between PIC simulations, analytical models and MD calculations for the first time but also unequivocally prove that AHR processes is a universal dominant collisionless mechanism of absorption in the short pulse regime or in the early time of longer pulses in clusters.

PACS numbers: 36.40.Gk, 52.25.Os, 52.50.Jm

## I. INTRODUCTION

Laser-driven atomic clusters absorb large fraction of laser energy compared to traditional solid and gas targets. Solid like overdense plasma density of a cluster and its smaller size (of a few nanometer) than the wavelength of 800 nm laser pulse (typically used in experiments) allow full penetration of laser field without its attenuation, contrary to micron-sized solids, leading to nearly 90% laser absorption in clusters [1].

After the irradiation of a cluster by a laser pulse of intensity  $> 10^{14}$  Wcm $^{-2}$ , individual atoms in the cluster are ionized (called inner ionization) and a nano-plasma is created. Subsequent interactions lead to absorption of laser energy by electrons and removal of those energetic electrons from the time-dependent cluster potential (called outer ionization). As an electron crosses the cluster boundary or leaves the cluster completely, a local electrostatic (ES) field due to charge non-neutrality develops. This ES field together with the laser field may lead to further inner ionization (called ionization ignition [2]) and creation of higher charge states which are forbidden by the laser field alone. Higher ionic charge states from rare gas clusters at a lower intensity than required for isolated atoms confirm the role of this ionization ignition. The electrostatic energy stored in the non-neutral nano-plasma (after some electrons are removed by laser) gets converted to ion kinetic energies through ion-ion Coulomb repulsion resulting MeV ions [1, 3–11] in experiments. KeV electrons [10–16], x-rays [17–20] and MeV neutrals [21] in experiments are the consequence of efficient coupling of laser energy with cluster.

Clearly, without the efficient electron acceleration, the subsequent ion acceleration, x-ray generation and neutral atom acceleration can not happen. Therefore, investigation of underlying physical process of coupling of laser energy with electrons is very important. For infrared lasers (800 nm wavelength or above) with intensities  $I_0 > 10^{16}$  Wcm $^{-2}$ , collisional process of absorption through electron-ion collision can be ne-

glected since it scales as  $\sim I_0^{-3/2}$ . However, collisionless process of absorption continues irrespective of the laser intensity and the wavelength as long as the plasma is overdense.

Among the various collisionless processes, linear resonance (LR) occurs when Mie-plasma frequency  $\omega_M(t)$  of the Coulomb expanding cluster meets the laser frequency  $\omega$ . In experiments, it is achieved by a pump-probe technique [22–24] where a pump pulse first ionizes the cluster,  $\omega_M(t)$  rises above  $\omega$ , subsequent outer ionization of electrons leads to cluster expansion causing decrease of  $\omega_M(t)$  towards  $\omega$ , and after a suitable delay (typically  $> 100$  fs) a probe pulse hits the expanding cluster to meet the LR condition  $\omega_M(t) \approx \omega$  [25]. However, to make this LR to happen at a later time, we need to remove as many electrons by a laser from the cluster potential in an early time. Otherwise Coulomb expansion is not possible. Therefore, one must know how those electrons absorb energy in an early time of a long pulse laser. For a short pulse, ionic background can not expand sufficiently,  $\omega_M(t)$  does not fall upto  $\omega$  to meet LR; *but* energy absorption by electrons still persists. Therefore, we concentrate on the mechanism of energy absorption in the short pulse regime which is also applicable for the early duration of a longer pulse much before the LR can happen.

The role of  $\vec{v} \times \vec{B}$  heating [26] as a collisionless mechanism is discriminated here by restricting the laser intensity below  $10^{17}$  Wcm $^{-2}$  where  $B$  field of the laser is negligible. One may surmise the “Brunel effect” or the “vacuum heating” as a probable collisionless process in the early time of interaction when plasma boundary is sharp [27]. Firstly, the “vacuum” as mentioned by Brunel may not be a real vacuum. Electrostatic field exists in the target vicinity (as we shall show here) that plays a crucial role for an electron’s dynamics before it is liberated from the target or directed into the target. It can not gain a net energy, unless there is any nonlinear interaction through the nonlinear space-charge field within the target and/or in the target vicinity. Therefore, the tautological name

“vacuum heating” is improper. According to Brunel’s original proposition [27], when an intense laser pulse strikes a sharply bounded overdense plasma; electrons are dragged in to the vacuum and then due to the laser field reversal, in the next half-cycle of the pulse, electrons are pushed back inside the target with a velocity on the order of the ponderomotive velocity  $v_0 = eE_0/m\omega$ . The *crucial* assumption in this model is that electrons experience *no net* field while they return to the target. As a consequence Brunel’s electron flow becomes laminar, meaning that their trajectories do not cross each other within a laser period irrespective of the laser intensity. We point out that, since different electrons originate from different parts of the target they experience different electrostatic fields and originate with different initial phases. When driven by a laser, their trajectory crossing is unavoidable at a later time. Detail analysis showing deficiency in Brunel’s “vacuum heating” is given in Ref.[28]. Brunel electrons, upon returning to the target, experience a field free region due to complete cancellation of induced electrostatic field by the laser field. Thus, the velocities acquired during their traversal in the vacuum are fully retained, they do not have chance to give energy back (even partly) to the electromagnetic field. In the context of laser-cluster interaction, induced electrostatic fields can not be fully compensated by the laser field (induced field may exceed the laser field) and cluster interior is rarely field free (as shown in this work) during the laser interaction. Otherwise, ionization ignition [2] can not happen and higher charge states [29–32] of ions can not be created. In this sense, Brunel effect is incomplete, warrant a re-look into the problem and search for an appropriate mechanism behind the laser absorption.

On the other hand, let us suppose that there is an anharmonic potential created at the target front (or in the target interior) due to the laser interaction. Such a potential is inevitably formed (for any finite size target) at the ion-vacuum boundary (where laser interacts first) due to  $\sim 1/r$  fall of the potential which may be asymmetric. Anharmonicity in the potential also appears due to local charge non-uniformity (via ionization, concentrated electron cloud etc.) in a laser driven plasma. The frequency  $\Omega$  of an electron in such a potential is dependent on its position  $r$ . When driven by a laser field, its  $r$  changes with time which makes  $\Omega(r)$  time dependent, i.e.,  $\Omega[r(t)]$ . An initially bound electron, starting from some location in the overdense plasma potential, while becoming free must experience the  $\sim 1/r$  Coulomb tail of the potential and the corresponding  $\Omega[r(t)]$  of the electron must meet  $\omega$  while trying to come out of the potential. This dynamical resonance - the anharmonic resonance (AHR) - occurring in an anharmonic potential was studied before using a model and three dimensional PIC simulations of laser driven clusters [33]. However, collisionless processes and AHR phenomenon remain to be a debate [28, 34, 35]. In numerical simulations it is often obscured due to many body nature of interaction, since it needs clear examination of individual electron trajectory, identification of corresponding  $\Omega[r(t)]$  and a dynamical mapping of  $\Omega[r(t)]$  on to  $\omega$ . To prove AHR for a laser driven cluster a three dimensional MD simulation code with soft-core Coulomb interactions among charge particles has been developed. By following the trajectory of each MD electron and

identifying its time-dependent frequency  $\Omega[r(t)]$  in the self-generated anharmonic plasma potential it is found that electron leaves the potential and becomes free only when AHR condition  $\Omega[r(t)] = \omega$  is met. Thus, for the first time, our MD simulation clearly identifies AHR process in the laser cluster interaction. We further introduce a non-linear oscillator model that brings out most of the features of MD electrons while passing the AHR. Thus, we bridge the gap between PIC simulations, analytical models and MD calculations.

Atomic units (i.e.,  $m_e = -e = 1, 4\pi\epsilon_0 = 1, \hbar = 1$ ) are used throughout this work unless specified explicitly. We consider a single deuterium cluster of radius  $R = 2.05$  nm, Wigner-seitz radius  $r_w = R/N^{1/3} \approx 0.17$  nm and number of atoms  $N = 1791$ . It is irradiated by 800 nm wavelength laser pulses of various intensity giving density  $\rho \approx 27.3\rho_c$  and  $\omega_p^2/3\omega^2 = \omega_M^2/\omega^2 \approx 9.24$ ; where  $\rho_c = \omega^2/4\pi$  is the critical density at 800 nm and  $\omega_p$  is the plasma frequency. These parameters of the cluster are kept unchanged throughout this work.

Section II illustrates AHR by a simple model of a cluster while Sec.III proves the hypothesis of AHR by detailed MD simulations. Summary and conclusion are given in Sec.IV.

## II. MODEL FOR ANHARMONIC RESONANCE ABSORPTION

Before studying the laser-cluster interaction by MD simulations, we show here various features of AHR by a model of a cluster which will provide an easy interpretation of MD results in Sec.III. In the model, cluster is assumed to be pre-ionized and consists of homogeneously charged spheres of massive ions and much lighter electrons of equal radii  $R_i = R_e = R$ . When their centers coincide plasma becomes charge neutral. The motion of ions can be neglected for short laser pulses  $< 50$  fs and non-relativistic laser intensities  $< 10^{18}$  Wcm $^{-2}$  as considered in this work. Thus ion sphere provides a sharp boundary with zero density gradient scale-length at the vacuum plasma boundary.

The equation of motion (EOM) of the electron sphere in a linearly polarized laser field along  $x$ -direction reads

$$\frac{d^2\vec{r}}{dt^2} + \frac{\vec{r}}{r}g(r) = \hat{x}(q_e/m_e)E_l(t) \quad (1)$$

where  $\vec{r} = \vec{x}/R$  and  $r = |\vec{r}|$ . The electrostatic restoring field

$$g(r) = \omega_M^2 R \times \begin{cases} r & \text{if } 0 \leq r \leq 1 \\ 1/r^2 & \text{if } r \geq 1, \end{cases} \quad (2)$$

can be derived by Gauss’s law. It shows that as long as the excursion  $r$  of the center of the electron sphere remains inside the ion sphere, it experience a harmonic oscillation with a constant eigen-frequency  $\omega_M$ . Crossing the boundary of the ion sphere, it begins to experience the Coulomb force and its motion becomes anharmonic with gradual reduction in the eigen-frequency for increasing excursion from the center of the ion sphere. The nonlinear restoring field (2) is simpler than used earlier [36, 37]. Nevertheless, it exhibits all features

AHR phenomena elegantly, e.g., prompt generation of electrons within a time much shorter than a laser period, crossing of electron trajectories and subsequent non-laminar electron flow [35]. It neglects the interaction of diffuse boundary of the electron sphere with the sharp boundary of the ion sphere, *but* allows us to calculate  $\Omega[r]$  of the electron sphere analytically for an arbitrary excursion which is not possible with the  $g(r)$  in Refs.[36, 37].

The cluster size being much smaller than the laser wavelength  $\lambda = 800$  nm as considered in this work, the dipole approximation for the laser vector potential  $A(z, t) = A(t) \exp(-i2\pi z/\lambda) \approx A(t)$  is assumed. Thus, the effect of propagation of light (directed in  $z$ ) is disregarded. We take  $A(t) = (E_0/\omega) \sin^2(\omega t/2n) \cos(\omega t)$  for  $0 < t < nT$ ; where  $n$  is the number of laser period  $T$ ,  $nT$  is the total pulse duration and  $E_0$  is the field strength corresponding to an intensity  $I_0 = E_0^2$ . The driving field  $E_I(t) = -dA/dt$  reads

$$E_I(t) = (E_0/\omega) \begin{cases} \sum_{i=1}^3 c_i \omega_i \sin(\omega_i t) & \text{if } 0 < t < nT \\ 0 & \text{otherwise;} \end{cases} \quad (3)$$

where  $c_1 = 1/2, c_2 = c_3 = -1/4, \omega_1 = \omega, \omega_2 = (1 + 1/n)\omega$ , and  $\omega_3 = (1 - 1/n)\omega$ . Eq.(3) leads to the correct dynamics of a free electron [38] even for very short sub-cycle pulses in contrast to the often used  $\sin^2$ -pulses [23, 39–41].

#### A. Effective frequency of the electron sphere

The electrostatic potential corresponding to Eq.(2) reads

$$\phi(r) = \omega_M^2 R^2 \times \begin{cases} 3/2 - r^2/2 & \text{if } 0 \leq r \leq 1 \\ 1/r & \text{if } r \geq 1. \end{cases} \quad (4)$$

In the absence of a driver, the eigen-period  $T$  of oscillation of the electron sphere in the potential (4) can be calculated from

$$T = \frac{4R}{\sqrt{2}} \int_0^{r_m} \frac{dr}{\sqrt{\Phi(r_m) - \Phi(r)}}. \quad (5)$$

Here  $\Phi(r_m) = q_e \phi(r_m)$  is the potential energy stored in the oscillator at an initial distance  $r = r_m$  from where it is left freely in the potential at a time  $t = 0$ . For  $0 \leq r_m \leq 1$ , Eq. (5) yields a constant  $T = 2\pi/\omega_M$  and the effective frequency of oscillation of the electronic sphere as

$$\Omega(r) = 2\pi/T = \omega_M. \quad (6)$$

When  $r_m > 1$ , we write  $T = T_1 + T_2$  with  $T_1/4$  as the time required for  $r = 1$  to  $r = 0$  and  $T_2/4 = \frac{R}{\sqrt{2}} \int_{r_m}^1 \frac{dr}{\sqrt{\Phi(r_m) - \Phi(r)}}$  is the time required for  $r = r_m$  to  $r = 1$  which give

$$T_1 = \frac{4}{\omega_M} \left[ \sin^{-1} \left( \sqrt{r_m/(3r_m - 2)} \right) \right],$$

$$T_2 = \frac{(2r_m)^{3/2}}{\omega_M} \left[ \sin^{-1} \left( \sqrt{(r_m - 1)/r_m} \right) + \sqrt{(r_m - 1)/r_m^2} \right]. \quad (7)$$

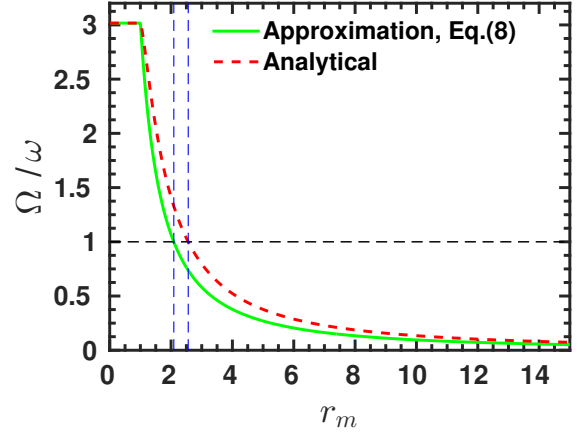


Figure 1. Normalized effective frequency  $\Omega/\omega$  of the electron sphere versus its excursion amplitude  $r_m$  for a deuterium cluster of radius  $R = 2.05$  nm, Wigner-seitz radius  $r_w \approx 0.17$  nm and number of atoms  $N = 1791$ , density  $\rho \approx 27.3\rho_c$  and  $\omega_M^2/\omega^2 \approx 9.24$ ; where  $\rho_c = \omega^2/4\pi$  is the critical density at  $\lambda = 800$  nm. Numerical approximation using Eq.(8) and the analytical result using Eqns.(6)-(7) are comparable. Vertical dashed lines indicate AHR is expected near  $r_m \approx 2$  according to Eq.(8) and  $r_m \approx 2.5$  according to Eq.(7).

$T_1$  is obtained from the harmonic solution  $r_{in} = \sqrt{R^2 + v_R^2/\omega_M^2} \sin(\omega_M(t - T_2/4) + \arctan(\omega_M R/v_R))$  inside the cluster satisfied by the electron that enters the surface of the cluster with the velocity  $v_R = -\omega_M R \sqrt{2(r_m - 1)/r_m}$  (obtained from the energy conservation) at  $t = T_2/4$ . If the electron starts at the surface of the cluster, i.e., at  $r_m = 1$ , we get  $T_1 = 2\pi/\omega_M$ ,  $T_2 = 0$  and recover Eq.(6) with  $T = T_1$ . The effective frequency  $\Omega(r) = 2\pi/(T_1 + T_2)$  now depends on the excursion amplitude  $r = r_m$ , since the electron sphere interacts with the nonlinear part of the restoring field. In a laser field excursion changes with time. Thus  $\Omega[r(t)]$  depends on  $t$  when  $r(t) > 1$ . In more realistic MD simulations of clusters, there is no pre-defined potential (as Eq.(4)) in which electrons oscillate. Therefore, finding  $\Omega(r)$  analytically is not possible in MD. From Eq. (1) we formally write (in analogy with a harmonic oscillator) the square of  $\Omega(r)$  as the ratio of restoring field to the excursion of the electron sphere [33]

$$\Omega^2[r(t)] = \frac{g[r(t)]}{r(t)} = \frac{\text{restoring field}}{\text{excursion}}. \quad (8)$$

Note that for a harmonic oscillator above relation yields the correct eigen frequency  $\Omega_h$  with  $g(r) = \Omega_h^2 r$ .

Analytical result of the normalized effective frequency  $\Omega/\omega$  using (Eqns.(6)-(7)) as a function of excursion ( $r_m$ ) of the electron sphere in the potential (4) is plotted in Fig. 1. Numerical solution of Eq. (1) (without the laser field) gives  $r(t)$  and corresponding  $\Omega/\omega$  from Eq. (8). This numerical approximation is also plotted in Fig. 1 which matches reasonably well with the analytical  $\Omega/\omega$ . As the electron sphere moves away from harmonic region of the potential,  $\Omega/\omega$  starts decreasing. At a distance of  $r_m \approx 2$ , the AHR condition  $\Omega/\omega \approx 1$  is satisfied. If the laser field is strong enough to bring the elec-

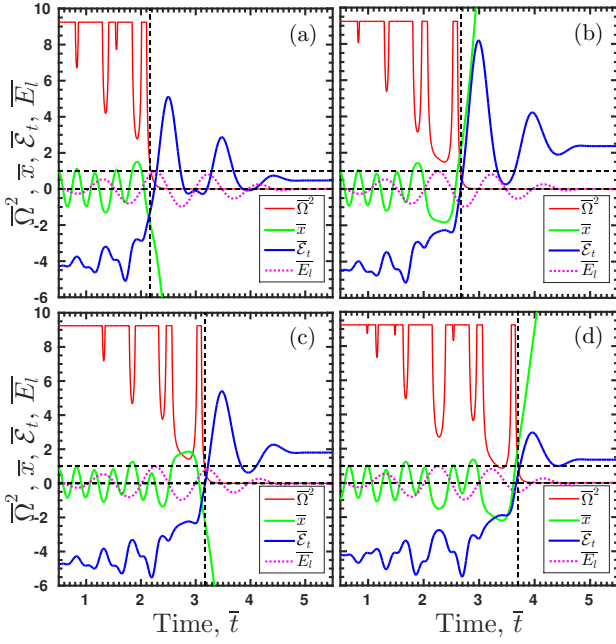


Figure 2. Normalized value of the square of the effective frequency  $\bar{\Omega}^2(r)$ , excursion  $\bar{x}$ , total energy  $\bar{\mathcal{E}}_t$  and the laser field  $\bar{E}_l$  versus the normalized time  $\bar{t} = t/T$  for four electron spheres undergoing AHR at successive times (a)  $\bar{t} = 2.2$ , (b)  $\bar{t} = 2.7$ , (c)  $\bar{t} = 3.2$ , (d)  $\bar{t} = 3.7$ . The deuterium cluster of Fig.1 is irradiated by a  $n = 5$ -cycle pulse of peak intensity  $5 \times 10^{15} \text{ W/cm}^2$ .

tron sphere at a value of  $r(t) = r_m \approx 2$ , the electron sphere may gain significant energy from the laser field via such AHR.

### B. Dynamics of the electron sphere in the laser field

The dynamical behaviour of the electron sphere (for the above cluster) irradiated by a  $n = 5$ -cycle pulse (3) of duration  $nT = 13.5 \text{ fs}$  and peak intensity  $5 \times 10^{15} \text{ W/cm}^2$  is now studied. Figure 2(a-d) depicts the normalized value of the square of the frequency  $\bar{\Omega}^2(r) = \Omega^2(r)/\omega^2$  using Eq.(8), excursion  $\bar{x} = x/R$ , total energy  $\bar{\mathcal{E}}_t = \mathcal{E}_t/U_p$  and the laser field  $\bar{E}_l = E_l/E_0$  versus the normalized time  $\bar{t} = t/T$  for the electron sphere placed at four different initial locations  $|\bar{x}| < 1$  in the potential. Initially, spheres are bound with different energies (near  $\bar{\mathcal{E}}_t \approx -4$ ) where they experience a constant frequency  $\Omega[r(0)] = \omega_M$ . Up to  $t/T \lesssim 2.0$ , in Fig.2(a), the laser field strength is not sufficient to liberate the electron sphere from the potential. In the oscillating laser field, at times  $\bar{x}$  exceeds unity with a decrease in  $\bar{\Omega}^2$  from  $\omega_M^2/\omega^2 \approx 9.24$  and the corresponding increase in  $\bar{\mathcal{E}}_t$ . The decrease of  $\bar{\Omega}^2[r(t)]$  being insufficient to meet the AHR condition  $\bar{\Omega}^2[r(t)] \approx 1$  (dashed horizontal line), particle can not absorb sufficient energy to come out completely but pulled back towards the potential center (see the reversal of  $\bar{x}$  and  $\bar{\Omega}^2$  near  $t/T \approx 1.9$ ) by the restoring force due to the ion sphere. As it reverses its direction and emerges on the other side of the potential with  $\bar{x} < 0$ ;

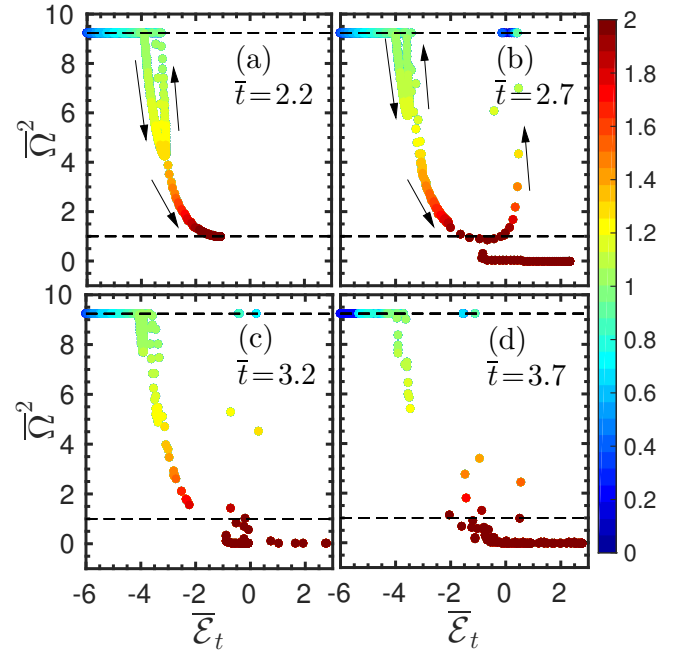


Figure 3. (color online) Snapshots of  $N = 1791$  non-interacting electron spheres in the  $(\bar{\mathcal{E}}_t, \bar{\Omega}^2)$  plane at times (a)  $\bar{t} = 2.2$ , (b)  $\bar{t} = 2.7$ , (c)  $\bar{t} = 3.2$ , (d)  $\bar{t} = 3.7$  corresponding to Fig.2. As the laser field strength increases with time, more and more electrons are drawn towards the line of AHR, i.e. dashed line at  $\bar{\Omega}^2 \approx 1$ . The parameters of laser and cluster are same as in Fig.2.

the increasing laser field towards its peak value (i.e.,  $\bar{E}_l \sim 1$ ) after  $t/T \approx 2.0$  helps  $|\bar{x}|$  to exceed unity with a fast drop of  $\bar{\Omega}^2$  for  $t/T > 2.1$ . Around  $t/T \approx 2.2$  (indicated by vertical dashed line),  $\bar{\Omega}^2$  meets the AHR condition with  $|\bar{x}| \approx 2$ . The fact that AHR truly occurs at an excursion  $|\bar{x}| \approx 2$  is in agreement with Fig.1. It also justifies the robustness of the formal approximation (Eq.(8)) for retrieving the effective frequency from the numerical model. After the AHR (i.e.,  $t/T > 2.2$ ) particle becomes completely free with  $\bar{\Omega}^2[r(t)] \approx 0$  and final energy  $\bar{\mathcal{E}}_t \geq 0$ .

Figures 2(c-d) show electron spheres undergoing AHR at  $t/T = 2.7, 3.2, 3.7$  respectively. Since initial positions are different, they have different initial phases and experience different restoring fields and total fields even though same laser field acts on them. As a result they are emitted at different times from the potential experiencing the AHR with different laser field strengths. Electron spheres experiencing AHR at a higher driving field strength generally acquire higher energies after the pulse as in Figs.2(a-c). Some electrons may also exhibit [as in Fig.2(d)] multiple AHR: they leave the cluster potential through AHR, return to the cluster interior by the laser field (or by the stronger restoring field than the laser field) and finally become free with a net positive energy via the AHR.

In this model electrons are frozen into a single sphere. Whereas, in reality, electrons in a cluster distinctly move even with a low intensity short laser pulse. Such a multi-electron system with all possible electrostatic interactions will be con-

sidered in detail by MD simulations in Sec.III. To gain some more physical insight on the dynamics of electrons in a multi-electron cluster and the AHR through the above model, we consider  $N = 1791$  non-interacting electron spheres (mimicking the multi-electron system) placed uniformly inside the ion sphere. Each electron sphere mimics a real point size electron.

Figures 3(a-d) show snapshots of all non-interacting electron spheres (each dot represents a sphere) in the energy versus effective frequency plane at times  $\bar{t} = 2.2, 2.7, 3.2, 3.7$  corresponding to Figs.2(a-d). Colors indicate their normalized positions.

In an early time  $t/T = 2.2$  [in Fig.3(a)] a large fraction of electrons are bound in the harmonic part of the potential with frequency  $\bar{\Omega}^2 = \omega_M^2/\omega^2 = 9.24$  and excursion  $r < 1$  (dark blue to light blue). Some electrons first come out of the harmonic part and continue in the anharmonic part of the potential with a drop in  $\bar{\Omega}^2$  (up to 4) and increasing excursion  $1 < r < 1.3$  (light green to yellow). But the restoring field on them being higher than the laser field they return to the cluster (see reversal of electrons with change of colors green-yellow-green in the U-shaped lobe) and become bound. At this time a few electrons (dark red to brown) are aligned towards the line of AHR (horizontal dashed line) with excursion  $r \approx 2$  and frequency  $\bar{\Omega} \approx 1$ . At a later time  $t/T = 2.7$  [in Figs.3(b)], phase of the laser field is reversed with nearly the same strength. Apart from bound and returning electrons [as in Fig.3(a)], it is clear that many electrons are now drawn towards the line of resonance, some are already free during this half laser cycles between  $t/T = 2.2 - 2.7$  due to change in the field. Beyond  $t/T = 2.5$  [in Figs.3(b-d)] laser field strength becomes weaker than the restoring field on some quasi-free electrons. Those electrons (typically having low energies) are dragged inside the cluster (see their color changes from brown to yellow) even though they were made free via the AHR earlier.

Thus a simple nonlinear oscillator model brings out most of the physics of AHR phenomena for a laser driven cluster in the temporal domain (Fig.2) as well as in the energy versus frequency domain (Fig.3). The identification of the effective dynamical frequency  $\Omega[r(t)]$  of the driven oscillator in the numerical model and the liberation of particles from the cluster potential only when  $\Omega$  matches the resonance condition  $\Omega \approx \omega$ , clearly justifies the robustness of the formal approximation in Eq.(8) and permits its application in the self-consistent MD simulations in Sec.III.

### III. ANHARMONIC RESONANCE ABSORPTION USING MOLECULAR DYNAMICS SIMULATION

It is mentioned that in the above model electrons are frozen in a sphere which moves in a predefined attractive potential due to the ion sphere. In reality, the potential of the ionized cluster varies with the time to time redistribution of charges. In the initial time, when cluster is charge neutral, potential must start from a zero value. Electrons may also face repulsive potential due to concentrated electron cloud in some part of the cluster. In the model, the electron sphere either stays inside (0% outer ionization) the cluster or completely goes

out of the cluster (100% outer ionization) for a given laser intensity. However, there is always a certain fraction of outer ionized electrons even at an intensity just above the inner ionization threshold. These shortcomings of the model can be addressed by MD simulation.

#### A. Details of molecular dynamics simulation

A three-dimensional MD simulation code is developed to study the interaction of laser light with cluster. Particular attention is given to the identification of AHR process using MD simulation. Cluster is assumed to be pre-ionized. This may be regarded as a situation where ionization has already taken place by a pump pulse and subsequent interaction of a probe pulse is studied. Electron-electron, ion-electron and ion-ion interactions through the Coulomb field are taken into account. Binary collisions among particles are neglected since we are interested in collisionless processes. The EOM of  $i$ -th particle in a laser field polarized in  $x$  and propagating in  $z$  (in the dipole approximation) reads

$$m_i \frac{d\vec{v}_i}{dt} = \vec{F}_i(r_i, v_i, t) + \hat{x} q_i E_l(t) + q_i \vec{v}_i \times \hat{y} B_l(t), \quad (9)$$

where  $\vec{F}_i = \sum_{j=1, i \neq j}^{N_p} q_i q_j \vec{r}_{ij} / r_{ij}^3$  is the Coulomb force on  $i$ -th particle of charge  $q_i$  due to all  $j$ -th particles each of charge  $q_j$  in the system.  $E_l(t)$  and  $B_l(t)$  are the electric and magnetic part of the laser field. Usually,  $B_l(t) \approx E_l(t)/c \ll 1$  for intensities  $< 10^{18} \text{ Wcm}^{-2}$ . To avoid steep increase in the Coulomb force  $\vec{F}_i$ , for a small separation  $r_{ij} \rightarrow 0$ , a smoothing parameter  $r_0$  is added with  $r_{ij}$ . The modified Coulomb force on  $i$ -th particle and the corresponding potential at its location are

$$\vec{F}_i = \sum_{j=1, i \neq j}^{N_p} \frac{q_i q_j \vec{r}_{ij}}{(r_{ij}^2 + r_0^2)^{3/2}}, \quad \phi_i = \sum_{j=1, i \neq j}^{N_p} \frac{q_j}{(r_{ij}^2 + r_0^2)^{1/2}}. \quad (10)$$

This modification of the force allows a charge particle to pass through another charge particle in the same way as in the PIC simulation. Thus it helps to study collisionless energy absorption processes in plasmas, e.g., resonances.

Equation (9) is solved using the velocity verlet time integration scheme [42] with a uniform time step  $\Delta t = 0.1 \text{ a.u.}$ . The code is validated by verifying the energy conservation of the system as well as identifying the electron plasma oscillation with desired Mie-plasma frequency  $\omega_M$  for the spherical cluster plasma. Although there are plenty of MD simulations for clusters [2, 30, 41, 43–58], verification of this natural oscillation through MD simulation is rarely reported which is extremely important, particularly to study frequency dependent phenomena, e.g., anharmonic and harmonic resonance absorption in laser driven plasmas. Otherwise, resonance physics may be missing in simulations and subsequent MD results could be misleading. In fact, MD codes in Refs.[47–50] could not find the signature of resonances in laser cluster interaction and the reason was unknown; while



experiments [25, 59–61], theory and particle-in-cell simulation [33, 36, 39, 40, 62–64] studies clearly indicated its importance.

We note that the artificial free parameter  $r_0$  in most of the earlier works has been chosen by considering *only* the energy conservation point of view in the simulation. In Refs.[43–45],  $r_0 = 0.02$  nm for electron-electron interaction and  $r_0 = 0.1$  nm for electron-ion interaction have been taken which do not violate the energy conservation in the case of xenon cluster. In Ref. [46],  $r_0 = 0.15$  nm for argon and  $r_0 = 0.12$  nm for xenon cluster were chosen such that the minimum of the electron-ion interaction potential agrees with the ionization potential of the neutral atom. MD codes in Refs. [47–53] have reported similar kind of  $r_0$  values as in Refs. [43–45]. Some of the authors have also chosen large  $r_0$  on the order of cluster radius [2, 54] and energy conservation is still obeyed.

In our simulation, frequency of oscillation ( $\omega_M$ ) of electrons is found to be sensitive on the value of the  $r_0$  while conservation of energy is obeyed even for larger values of  $r_0$ . But energy conservation *alone* can not grant correctness of particle dynamics in simulations. To get correct oscillation frequency ( $\omega_M$ ) one can not choose  $r_0$  arbitrarily and a law has to be enforced. For a very small separation  $r_{ij} \ll r_0$ , the space charge field on the  $i$ -th particle  $\vec{E}_i^{sc} = \vec{F}_i/q_i$  has to be linear in  $r_{ij}$  and its slope has to be  $\omega_M^2$ , i.e.,  $\vec{E}_i^{sc} = \vec{F}_i/q_i = \omega_M^2 \vec{r}_{ij}$  in order to get correct plasma oscillations. From Eq.(10), we find that  $\vec{E}_i^{sc} = \vec{F}_i/q_i \approx \sum_j (q_j/r_0^3) \vec{r}_{ij} \approx (Q_0/r_0^3) \vec{r}_{ij}$  for  $r_{ij} \ll r_0$ ; assuming  $Q_0$  is the total uniformly distributed charge of type  $j$  inside the sphere of radius  $r_0$  where all  $r_{ij}$  are nearly same for collective plasma oscillations. From the above two expressions of space-charge field  $\vec{E}_i^{sc} = \omega_M^2 \vec{r}_{ij}$  and  $\vec{E}_i^{sc} \approx (Q_0/r_0^3) \vec{r}_{ij}$  we get  $\omega_M^2 = Q_0/r_0^3$ . For uniform ionic charge density  $\rho$  we write  $\rho = Q/(4\pi/3)R^3 = Q_0/(4\pi/3)r_0^3$  which gives  $Q/r_0^3 = Q_0/r_0^3 = 4\pi\rho/3 = \omega_M^2$ . Thus we get  $Q_0/r_0^3 = N_0Z/r_0^3 = Q/R^3 = NZ/R^3$  and  $r_0 = R(N_0/N)^{1/3}$ ; where  $Z$  is the uniform charge state of ions in the cluster,  $N_0, N$  are the number of ions inside the sphere of radius  $r_0$  and  $R$ ,  $Q_0 = N_0Z, Q = NZ$  are the total ionic charge in the sphere of radius  $r_0$  and in the cluster respectively. At this point  $N_0$  remains arbitrary. We note that  $r_0$  should be as small as possible, but non-zero. For a non-zero ionic charge density there should be at least one ion (to provide the restoring force to an electron) in the sphere of radius  $r_0$ . Therefore, setting  $N_0 = 1$ , we find that  $r_0 = R/N^{1/3}$  is the most legitimate choice [55] which is equal to the well known Wigner-Seitz radius  $r_w = R/N^{1/3}$  for a given cluster that leads to correct Mie-plasma oscillation if the law of force is of Coulombic in nature.

To prove that our MD code is capable of producing oscillation of electrons at the Mie-plasma frequency in the absence of a laser field, the deuterium cluster of radius  $R = 2.05$  nm, and number of atoms  $N = 1791$  (as in Sec.II) is considered. To make homogeneously charged positive background in which electrons will oscillate, all  $N_i$  ions ( $N_i = N = 1791$ ) are uniformly distributed initially. It gives ionic charge density  $\rho_i = 0.007$  a.u. and  $\omega_M = \sqrt{4\pi\rho_i/3} = 0.1735$  a.u.. A fewer number of  $N_e$  electrons (forming a homogeneous sphere of radius  $R/2$ ) is uniformly and symmetrically distributed about the center of

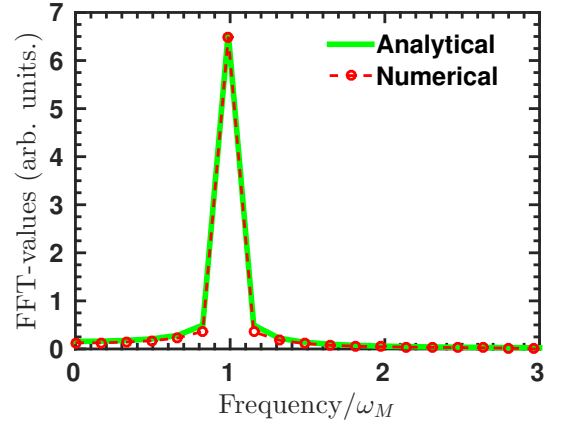


Figure 4. (color online) FFT of the center of mass (CM) position coordinate of electrons for a deuterium cluster of radius  $R = 2.05$  nm, and number of atoms  $N = 1791$ . Frequency is normalized by  $\omega_M$ . MD simulation result (numerical, dashed-circle) matches with the analytical result (solid line) for the entire range of frequency.

the spherical ion background and the whole system is at rest. This may represent a situation when most of the electrons are removed from the cluster by a laser field, and the remaining cold electrons occupying the central region collectively oscillate with the frequency  $\omega_M$ . Electrons are now uniformly shifted (small perturbation) from the ionic background along  $x$ . The space charge field due to the local charge imbalance acts like a restoring field. Whether these electrons will oscillate at  $\omega_M$  is determined by the homogeneity of the charge density  $\rho_i$  and the linearity of the restoring field decided by the amount of perturbation. These are ensured by making the ion background homogeneous and keeping perturbation small so that electrons do not cross the cluster boundary. Under this condition one may write EOM of the center of mass of the electron cloud as  $\ddot{x} = \omega_M^2 x$ , giving  $x = x_0 \cos(\omega_M t)$  with initial conditions  $x(0) = x_0, \dot{x}(0) = 0$ ; and verify the MD simulation results.

The Fourier transform (FT) of the center of mass position  $X_{cm}(t) = \sum_1^{N_e} m_e x_i(t)/N_e$  of MD electrons gives the collective oscillation frequency of the electron cloud which is plotted with the FT of the analytical solution  $x = x_0 \cos(\omega_M t)$  in Fig. 4 after the normalization by  $\omega_M$ . An excellent match between the numerical (dashed-circle) and analytical (solid line) results confirms the collective oscillation of electrons at the Mie-plasma frequency by MD simulations. Extensive simulations have been performed for other values of  $r_0 = 0.5r_w, 2r_w, 3r_w, 4r_w$  to check the effect of  $r_0$  on the plasma oscillation dynamics. As time progresses, we find 5-20% reduction in the amplitude of plasma oscillation with 5 – 10% elongation in the plasma period compared to the case of  $r_0 = r_w$  and the desired analytical solution shown in Fig.4.

## B. Laser energy absorption and outer ionization

The MD code is now used to study interaction of  $n = 5$ -cycle laser pulse of duration  $nT = 13.5$  fs with the deuterium

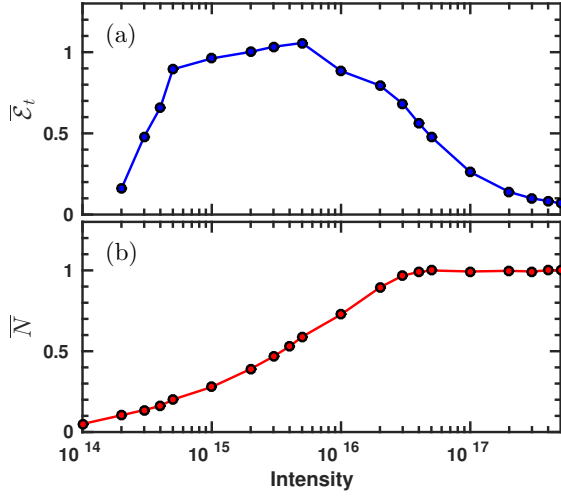


Figure 5. (color online) Total absorbed energy per electron in units of  $U_p$  (top) and fractional outer ionization (bottom) versus the laser intensity for a deuterium cluster of radius  $R = 2.05$  nm, and number of atoms  $N = 1791$ , density  $\rho \approx 27.3\rho_c$  and  $\omega_M^2/\omega^2 \approx 9.24$ . Cluster is illuminated by a  $n = 5$ -cycle laser pulse of wavelength 800 nm and various peak intensity.

cluster as in Sec.II. Initially, cluster has equal number of uniformly distributed ions and electrons (i.e.,  $N_i = N_e = N$ ) so that it is macroscopically charge neutral.

Figure 5 shows total absorbed energy per electron normalized by of  $U_p$  and corresponding degree of outer ionization at the end of the laser pulse as the peak intensity is varied. Normalized absorption per electron [in Fig.5(a)] attains a maximum between intensities  $5 \times 10^{15} - 10^{16} \text{ Wcm}^{-2}$ . This non-linear variation of absorbed energy with intensity is similar to that reported earlier using PIC simulations [33] of xenon clusters. The outer ionized fraction [in Fig.5(b)] of electrons, on the other hand, increases gradually with the peak intensity and saturates at unity (%100 outer ionization) at some higher intensity even for this short 5-cycle pulse. At an intensity  $5 \times 10^{15} \text{ Wcm}^{-2}$ , it is inferred that almost 60% electrons are outer ionized ( $\bar{N} \approx 0.6$ ) which contribute to the total absorbed energy of  $\approx 2000 U_p$ .

### C. Analysis of electron trajectory and finding the AHR

The high level of absorption and outer ionization shown in Fig.5 with a short 13.5 fs laser pulse is certainly not due to the linear resonance process. Figures 6(a-b) show normalized space charge field  $\bar{E}_x^{sc} = E_x^{sc}(t)/E_0$  and the total field  $\bar{E}_x^t = E_x^t(t)/E_0$  versus excursion  $\bar{x}(t)$  of a few selected outer ionized electrons (only 29 electrons are plotted) at the peak intensity  $5 \times 10^{15} \text{ Wcm}^{-2}$  of Fig.5. Corresponding  $\bar{x}(t)$  versus  $\bar{t}$  are shown in Fig.6(c). The crossing of trajectories of MD electrons [in Fig.6(c)] emitted from the cluster at different times, their non-laminar motion in time, the uncompensated laser field by the space charge field [in Fig.6(a)] and the corresponding non-zero total field [in Fig.6(b)] inside the clus-

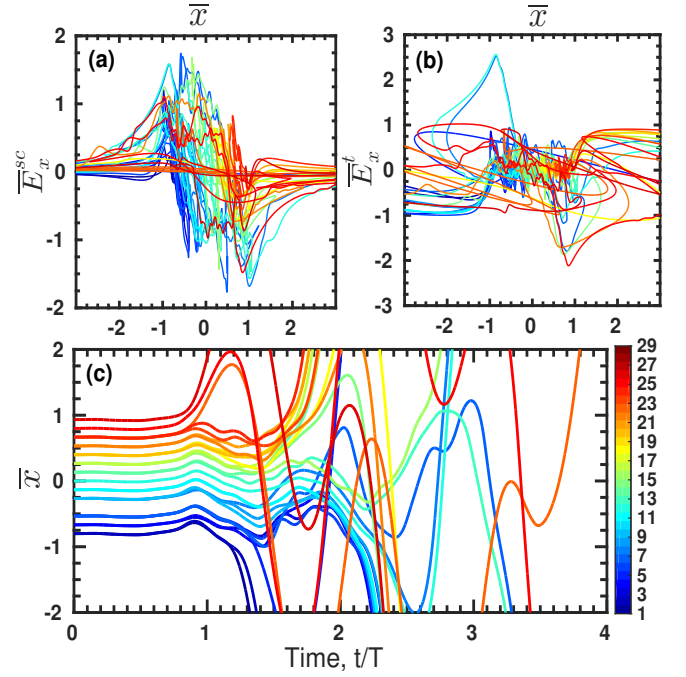


Figure 6. (color online) (a) Normalized self-generated space-charge field ( $E_x^{sc}(t)/E_0$ ) and (b) normalized total field ( $E_x^t(t)/E_0$ ) versus normalized excursion  $\bar{x}(t)/R$  of a few selected outer ionized electrons (only 29 electrons out of  $N = 1791$  are plotted, color bar indicates their index  $i = 1 - 29$ ) at a peak intensity of  $5 \times 10^{15} \text{ Wcm}^{-2}$ . Corresponding trajectories  $\bar{x}(t)/R$  versus  $t/T$  are shown in (c). All other the parameters of cluster and the laser are same as in Fig 5.

ter ( $-1 \leq \bar{x} \leq 1$ ) clearly suggest that absorption is not due the celebrated Brunel effect [27]. The underlying mechanism can be understood by analyzing trajectories of those MD electrons and finding the corresponding effective frequency as shown by the model in Sec.II B. We write the time dependent frequency of the  $i$ -th MD electron (in analogy with Eq.(8)) as

$$\Omega^2[r_i(t)] = \frac{\vec{E}_i^{sc}(\mathbf{r}_i, t) \cdot \mathbf{r}_i}{r_i^2} = \frac{\text{restoring field}}{\text{excursion}} \quad (11)$$

where  $\vec{E}_i^{sc} = \vec{F}_i/q_i$  is the electrostatic field on the  $i$ -th MD electron obtained from Eq. (10).

Figures 7(a-b) show different normalized quantities, i.e., frequency squared  $\bar{\Omega}^2$ , excursion  $\bar{x}$ , total energy  $\bar{\mathcal{E}}_i$ , laser field  $\bar{E}_l$  versus normalized time  $\bar{t}$  for selected MD electrons which are outer ionized at times: (a)  $\bar{t} = 1.1$  and (b)  $\bar{t} = 2.2$  from the cluster irradiated by the same 5-cycle laser pulse of peak intensity  $5 \times 10^{15} \text{ Wcm}^{-2}$ . Initially, the cluster is charge neutral, electrostatic field is zero inside the cluster and all particles are at rest. As a result, the effective frequency  $\Omega[r(t)]$  and total energy  $\mathcal{E}_i$  of each electron is zero. As the laser field is switched on, the charge separation potential and the corresponding field are dynamically created due to the movement of more mobile electrons than the slow moving ions. The MD electron in Fig.7(a) is first attracted inside such potential by the restoring force due to ions (see its excursion  $|\bar{x}|$  decreases towards the center of the cluster and total energy starts be-

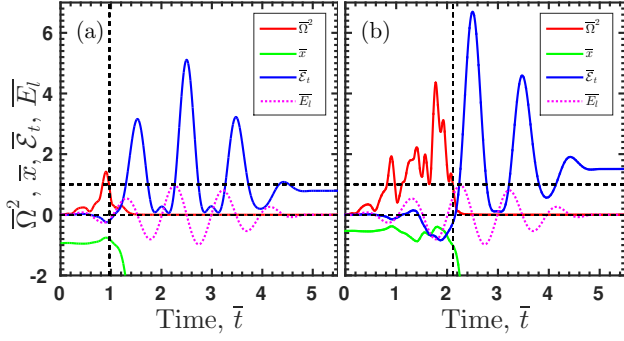


Figure 7. (color online) Normalized value of the square of the effective frequency  $\bar{\Omega}^2(r)$ , excursion  $\bar{x}$ , total energy  $\bar{\mathcal{E}}_t$  and the laser field  $\bar{E}_l$  versus the normalized time  $\bar{t}$  for different MD electrons undergoing AHR and outer ionization at times (a)  $\bar{t} = 1.1$ , (b)  $\bar{t} = 2.2$ . The cluster is irradiated by a  $n = 5$ -cycle pulse of peak intensity  $5 \times 10^{15} \text{ W/cm}^2$ . These results resemble with the results of model analysis in Fig. 2.

coming negative) where its effective frequency  $\Omega[r(t)]$  after increasing from zero exceeds the laser frequency  $\omega$  and goes to a maximum value when its total energy reaches a minimum negative value (i.e., it becomes more bound in the potential). From this point onwards the dynamics of the MD electron is very similar to the electron sphere in the model. As the laser field changes further, electron is pulled towards the negative  $x$ -direction,  $|\bar{x}|$  increases beyond unity,  $\bar{\Omega}^2$  drops from its maximum and crosses the line of AHR (horizontal dashed line where  $\bar{\Omega}^2 = 1$ ) near  $t/T \approx 0.95$  with the corresponding increase in  $\bar{\mathcal{E}}_t$  from negative to positive value (bound to free motion) similar to that shown in Fig. 2 using the model. After the AHR, electron leaves the cluster forever with a total energy of  $0.8U_p$  in the end of the pulse. In this early time of interaction, the laser field being very weak, only the loosely bound outer most electrons as compared to the core electrons leave the cluster. Such early leaving electrons which experience AHR in a shallower potential with a low laser field strength generally carry low kinetic energies.

As the laser field increases to its peak value, more electrons are outer ionized from the core of the cluster [as in Fig. 7(b)]. They experience a relatively deeper potential. Electrons while moving in deep potentials have relatively higher  $\Omega[r(t)]$  [clear from 7(b)] and they require higher field strengths for their liberation. Indeed, MD electron in Fig. 7(b) becomes free when its  $\bar{\Omega}^2$  passes the resonance line  $\bar{\Omega}^2 = 1$  after dropping from its maximum value and its energy  $\bar{\mathcal{E}}_t$  becomes positive at  $\bar{t} \approx 2.2$  as the peak of the pulse is approached.

The occurrence of AHR for MD electrons in Fig. 7 resemble with Fig. 2 in the model in Sec. II except that frequency and potential start from zero and self-consistently generated in the case of MD while those are predefined in the model.

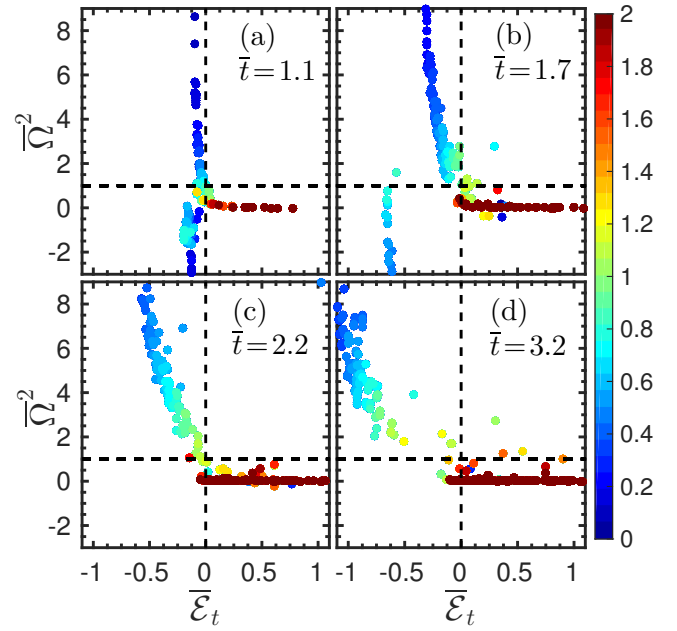


Figure 8. (color online) Snapshots all MD electrons in the  $(\bar{\mathcal{E}}_t, \bar{\Omega}^2)$  plane at times (a)  $\bar{t} = 1.1$ , (b)  $\bar{t} = 1.7$ , (c)  $\bar{t} = 2.2$ , (d)  $\bar{t} = 3.2$ . As the laser field strength increases with time, more and more electrons are drawn towards the line of AHR, i.e., dashed line at  $\bar{\Omega}^2 \approx 1$ . The parameters of laser and cluster are same as in Fig. 7.

### 1. AHR in the frequency vs energy plane

To prove that all MD electrons essentially pass through AHR during their outer ionization, Figures 8(a-d) show snapshots of all electrons in the  $(\bar{\Omega}^2, \bar{\mathcal{E}}_t)$  plane at different times  $\bar{t} = 1.1, 1.7, 2.2, 3.2$  respectively. Colors indicate normalized positions ( $r$ ) of those electrons as in the Fig. 3. From Fig. 8 it is clear that each electron leaves the cluster ( $r > 1$ , green to dark red) and its energy becomes positive *only* when it crosses the line of AHR (dashed horizontal line at  $\bar{\Omega}^2 = 1$ ). After becoming free, electrons have zero effective frequency as they are beyond the influence of the electrostatic field.

In the early time  $\bar{t} = 1.1$ , in Fig. 8(a), only few electrons are outer ionized from the cluster and the resulting potential is shallow. As a result energies ( $\bar{\mathcal{E}}_t$ ) of the bound electrons are very close to zero but negative. Some of the bound electrons have negative  $\bar{\Omega}^2$  due to the repulsion of the compressed electron cloud in their vicinity at this early time.

At later times  $\bar{t} = 1.7, 2.2$ , in Figs. 8(b)-(c), as the laser field approaches its peak value, an increasing number of electrons are outer ionized via the AHR channel. As a result the potential depth gradually increases, remaining bound electrons move to a deeper potential due to the gradually stronger attractive force of the uncompensated bare ionic background, the population of negative  $\bar{\Omega}^2$  valued electrons moves gradually to the attractive potential (repulsion vanishes with increasing potential depth) and becomes almost negligible in Fig. 8(c) where all bound electrons are aligned to pass the AHR in the next time interval.



After the peak of the laser pulse, e.g., at  $\bar{t} = 3.2$  in Fig.8(d), since outer ionization is mostly saturated and the potential has already reached to its near maximum depth at the pulse peak before (i.e., near  $\bar{t} = 2.5$ ), many bound electrons are dragged into the potential (they have more negative energies) due to the weakening of the laser field compared to the attractive force due to ions. Some of the quasi-free electrons (electrons with positive  $\bar{\Omega}^2$  and positive  $\bar{\mathcal{E}}_i$ ) near the cluster boundary also return inside due to such attraction.

The feature of AHR shown in Fig.8 in the frequency versus energy plane resembles Fig.3 obtained by the model, except that some MD electrons in Fig.8 experience negative frequencies due to repulsion of the neighbouring electrons.

Above analysis of trajectories of MD electrons in the self-generated, time-varying potential clearly indicates that the passage of AHR is must during their outer ionization. The fact that large amount of energy absorption by an electron and its simultaneous liberation from the dynamical potential happening at the same time *only* when AHR condition is met, clearly proves the AHR as a responsible mechanism behind this efficient laser absorption in a cluster.

#### IV. SUMMARY AND CONCLUSION

The goal of this work is to re-examine the AHR absorption mechanism of intense infrared laser pulses in a over-dense cluster using MD simulations. Although, AHR was proved earlier by a rigid sphere model and particle-in-cell (PIC) simulations [33] of clusters, it still remains obscure in many-body plasma simulations. To prove AHR on a firm footing a three

dimensional MD simulation code with soft-core Coulomb interactions among charge particles has been developed. By following the trajectory of each individual MD electron and identifying its time-dependent frequency  $\Omega[r(t)]$  in the self-consistent anharmonic potential (as in Ref.[33]) it is found that electron leaves the potential and becomes free only when AHR condition  $\Omega[r(t)] = \omega$  is met. Thus, for the first time, our MD simulation clearly identifies AHR process in the laser cluster interaction. A simple anharmonic oscillator model is introduced to understand MD results better. The model brings out most of the features of MD electrons while passing the AHR. Thus, we not only bridge the gap between PIC simulations, analytical models and MD calculations but also unequivocally prove that AHR processes is a universal dominant collisionless mechanism of absorption in the short pulse regime or in the early time of longer pulses in clusters.

We believe that AHR mechanism works irrespective of the target size at least in the first few nano-layer of the sharp overdense plasma (zero density scale-length) where laser interacts first and the analysis of electron trajectories presented here may be useful to identify AHR in such targets.

The prompt generation of electrons via AHR within a time much shorter than a laser period, the crossing of electron trajectories [in Fig.6(c)] demonstrated by MD simulations and the breaking of laminar flow of electrons may lead to plasma wave-breaking and subsequent mixing of wave-phases [35] even at sub-relativistic laser intensities in an extended plasma.

#### ACKNOWLEDGMENTS

Authors would like to thank Sudip Sengupta for careful reading of the manuscript and providing useful suggestions.

- 
- [1] T. Ditmire, R. A. Smith, J. W. G. Tisch, and M. H. R. Hutchinson, Phys. Rev. Lett. **78**, 3121 (1997).
  - [2] C. Rose-Petruck, K. J. Schafer, K. R. Wilson, and C. P. J. Barty, Phys. Rev. A **55**, 1182 (1997).
  - [3] T. Ditmire, J. W. G. Tish, E. Springate, M. B. Mason, N. Hay, J. P. Marangos, and M. H. R. Hutchinson, Nature (London) **386**, 54 (1997).
  - [4] T. Ditmire, J. W. G. Tisch, E. Springate, M. B. Mason, N. Hay, J. P. Marangos, and M. H. R. Hutchinson, Phys. Rev. Lett. **78**, 2732 (1997).
  - [5] V. Kumarappan, M. Krishnamurthy, and D. Mathur, Phys. Rev. Lett. **87**, 085005 (2001).
  - [6] M. Lezius, S. Dobosz, D. Normand, and M. Schmidt, Phys. Rev. Lett. **80**, 261 (1998).
  - [7] Y. Fukuda, K. Yamakawa, Y. Akahane, M. Aoyama, N. Inoue, H. Ueda, and Y. Kishimoto, Phys. Rev. A **67**, 061201 (2003).
  - [8] V. Kumarappan, M. Krishnamurthy, D. Mathur, and L. C. Tribedi, Phys. Rev. A **63**, 023203 (2001).
  - [9] M. Krishnamurthy, D. Mathur, and V. Kumarappan, Phys. Rev. A **69**, 033202 (2004).
  - [10] V. Kumarappan, M. Krishnamurthy, and D. Mathur, Phys. Rev. A **66**, 033203 (2002).
  - [11] T. Ditmire, E. Springate, J. W. G. Tisch, Y. L. Shao, M. B. Mason, N. Hay, J. P. Marangos, and M. H. R. Hutchinson, Phys. Rev. A **57**, 369 (1998).
  - [12] E. Springate, N. Hay, J. W. G. Tisch, M. B. Mason, T. Ditmire, M. H. R. Hutchinson, and J. P. Marangos, Phys. Rev. A **61**, 063201 (2000).
  - [13] E. Springate, S. A. Aseyev, S. Zamith, and M. J. J. Vrakking, Phys. Rev. A **68**, 053201 (2003).
  - [14] Y. L. Shao, T. Ditmire, J. W. G. Tisch, E. Springate, J. P. Marangos, and M. H. R. Hutchinson, Phys. Rev. Lett. **77**, 3343 (1996).
  - [15] L. M. Chen, J. J. Park, K. H. Hong, I. W. Choi, J. L. Kim, J. Zhang, and C. H. Nam, Physics of Plasmas **9**, 3595 (2002).
  - [16] V. Kumarappan, M. Krishnamurthy, and D. Mathur, Phys. Rev. A **67**, 043204 (2003).
  - [17] J. Jha, D. Mathur, and M. Krishnamurthy, Journal of Physics B: Atomic, Molecular and Optical Physics **38**, L291 (2005).
  - [18] J. Jha, D. Mathur, and M. Krishnamurthy, Applied Physics Letters **88**, 041107 (2006).
  - [19] L. M. Chen, F. Liu, W. M. Wang, M. Kando, J. Y. Mao, L. Zhang, J. L. Ma, Y. T. Li, S. V. Bulanov, T. Tajima, Y. Kato, Z. M. Sheng, Z. Y. Wei, and J. Zhang, Phys. Rev. Lett. **104**, 215004 (2010).
  - [20] A. McPherson, B. D. Thompson, A. B. Borisov, K. Boyer, and C. K. Rhodes, Nature **370**, 631 (1994).
  - [21] R. Rajeev, T. M. Trivikram, K. P. M. Rishad, V. Narayanan, E. Krishnakumar, and M. Krishnamurthy, Nat Phys. **9**, 185 (2013).

- [22] J. Zweiback, T. Ditmire, and M. D. Perry, *Phys. Rev. A* **59**, R3166 (1999).
- [23] U. Saalmann, C. Siedschlag, and J. M. Rost, *Journal of Physics B: Atomic, Molecular and Optical Physics* **39**, R39 (2006).
- [24] T. Fennel, K.-H. Meiwes-Broer, J. Tiggesbäumker, P.-G. Reinhard, P. M. Dinh, and E. Suraud, *Rev. Mod. Phys.* **82**, 1793 (2010).
- [25] T. Ditmire, T. Donnelly, A. M. Rubenchik, R. W. Falcone, and M. D. Perry, *Phys. Rev. A* **53**, 3379 (1996).
- [26] W. L. Kruer and K. Estabrook, *Physics of Fluids* **28**, 430 (1985).
- [27] F. Brunel, *Phys. Rev. Lett.* **59**, 52 (1987).
- [28] P. Mulser, S. M. Weng, and T. Liseykina, *Physics of Plasmas* **19**, 043301 (2012).
- [29] D. Bauer and A. Macchi, *Phys. Rev. A* **68**, 033201 (2003).
- [30] K. Ishikawa and T. Blenski, *Phys. Rev. A* **62**, 063204 (2000).
- [31] D. Bauer, *Journal of Physics B: Atomic, Molecular and Optical Physics* **37**, 3085 (2004).
- [32] F. Megi, M. Belkacem, M. A. Bouchene, E. Suraud, and G. Zwicknagel, *Journal of Physics B: Atomic, Molecular and Optical Physics* **36**, 273 (2003).
- [33] M. Kundu and D. Bauer, *Phys. Rev. Lett.* **96**, 123401 (2006).
- [34] J. P. Geindre, R. S. Marjoribanks, and P. Audebert, *Phys. Rev. Lett.* **104**, 135001 (2010).
- [35] T. Liseykina, P. Mulser, and M. Murakami, *Physics of Plasmas* **22**, 033302 (2015).
- [36] M. Kundu and D. Bauer, *Phys. Rev. A* **74**, 063202 (2006).
- [37] S. V. Popruzhenko, M. Kundu, D. F. Zaretsky, and D. Bauer, *Phys. Rev. A* **77**, 063201 (2008).
- [38] M. Kundu, P. K. Kaw, and D. Bauer, *Phys. Rev. A* **85**, 023202 (2012).
- [39] P. Mulser, M. Kanopathipillai, and D. H. H. Hoffmann, *Phys. Rev. Lett.* **95**, 103401 (2005).
- [40] P. Mulser and M. Kanopathipillai, *Phys. Rev. A* **71**, 063201 (2005).
- [41] U. Saalmann and J.-M. Rost, *Phys. Rev. Lett.* **91**, 223401 (2003).
- [42] L. Verlet, *Phys. Rev.* **159**, 98 (1967).
- [43] I. Last and J. Jortner, *Phys. Rev. A* **60**, 2215 (1999).
- [44] I. Last and J. Jortner, *Phys. Rev. A* **62**, 013201 (2000).
- [45] I. Last and J. Jortner, *The Journal of Chemical Physics* **120**, 1336 (2004).
- [46] S. V. Fomichev, D. F. Zaretsky, D. Bauer, and W. Becker, *Phys. Rev. A* **71**, 013201 (2005).
- [47] G. M. Petrov, J. Davis, A. L. Velikovich, P. C. Kepple, A. Dasgupta, R. W. Clark, A. B. Borisov, K. Boyer, and C. K. Rhodes, *Phys. Rev. E* **71**, 036411 (2005).
- [48] G. M. Petrov, J. Davis, A. L. Velikovich, P. Kepple, A. Dasgupta, and R. W. Clark, *Physics of Plasmas* **12**, 063103 (2005).
- [49] G. M. Petrov and J. Davis, *Physics of Plasmas* **13**, 033106 (2006).
- [50] J. Davis, G. M. Petrov, and A. Velikovich, *Physics of Plasmas* **14**, 060701 (2007).
- [51] G. Mishra, A. R. Holkundkar, and N. Gupta, *Laser and Particle Beams* **29**, 305 (2011).
- [52] G. Mishra and N. K. Gupta, *Physics of Plasmas* **19**, 093107 (2012).
- [53] R. Cheng, C. Zhang, L.-B. Fu, and J. Liu, *Journal of Physics B: Atomic, Molecular and Optical Physics* **48**, 035601 (2015).
- [54] A. R. Holkundkar, G. Mishra, and N. K. Gupta, *Physics of Plasmas* **18**, 053102 (2011).
- [55] F. Greschik, L. Arndt, and H.-J. Kull, *EPL (Europhysics Letters)* **72**, 376 (2005).
- [56] O. Batishchev, A. Batishcheva, V. Bychenkov, C. Albukrek, A. Brantov, and W. Rozmus, *Computer Physics Communications* **164**, 53 (2004).
- [57] R. G. Bystryi and I. V. Morozov, *Journal of Physics B: Atomic, Molecular and Optical Physics* **48**, 015401 (2015).
- [58] M. Arbeiter and T. Fennel, *Phys. Rev. A* **82**, 013201 (2010).
- [59] T. Döppner, T. Fennel, T. Diederich, J. Tiggesbäumker, and K. H. Meiwes-Broer, *Phys. Rev. Lett.* **94**, 013401 (2005).
- [60] L. Köller, M. Schumacher, J. Köhn, S. Teuber, J. Tiggesbäumker, and K. H. Meiwes-Broer, *Phys. Rev. Lett.* **82**, 3783 (1999).
- [61] S. Zamith, T. Martchenko, Y. Ni, S. A. Aseyev, H. G. Muller, and M. J. J. Vrakking, *Phys. Rev. A* **70**, 011201 (2004).
- [62] T. Taguchi, T. M. Antonsen, and H. M. Milchberg, *Phys. Rev. Lett.* **92**, 205003 (2004).
- [63] T. M. Antonsen, T. Taguchi, A. Gupta, J. Palastro, and H. M. Milchberg, *Physics of Plasmas* **12**, 056703 (2005).
- [64] I. Kostyukov and J.-M. Rax, *Phys. Rev. E* **67**, 066405 (2003).